Wollastonite-Reinforced Polypropylene Composites Modified With Novel Metallocene EPR Copolymers. I. Phase Structure and Morphology

Iztok Švab,[1,2] **Vojko Musil,**[1] **Anđela Pustak,**[3] **Ivan Šmit**[3]
[1]*Institute of Technology, University of Maribor, FEB Maribor, 2000 Maribor, Slovenia*

[2]*ISOKON, Production and Processing of Thermoplastics Ltd., Mestni Trg 5a, 3210 Slovenske Konjice, Slovenia*

[3]*Ruđer Bošković Institute, 10002 Zagreb, Croatia*

Supermolecular structure of isotactic polypropylene/wollastonite/metallocene propylene–ethylene copolymers (iPP/W/EPR) composites was studied as a function of elastomer content (from 0 to 20 vol%) by optical, scanning, and transmission electron microscopy, wide-angle X-ray diffraction, and differential scanning calorimetry. Both, wollastonite and dispersed EPR particles, homogeneously incorporated into the iPP matrix, and affected the final phase structure and morphology of the iPP/wollastonite/EPR composites. Wollastonite particles were orientated plane-parallel to the sample surface and hindered spherulite growth of the iPP matrix. EPRs enhanced plane-parallel orientation of wollastonite and simultaneously enhanced the spherulite and crystallite growth in the iPP matrix during the solidification of polymer melt. Ternary iPP/wollastonite/EPR composites exhibited significant prevalence of separated microphase morphology (over core-shell morphology) because of constitution similarity of P-E and iPP chains. POLYM. COMPOS., 30:1007–1015, 2009. © 2008 Society of Plastics Engineers

INTRODUCTION

Blending of polymers or compounding polymers with different fillers is a rather simple way to produce new polymeric materials with desired properties. Production and use of particulate-filled polymer composites have increased intensively because of favorable cost/performance ratio. The cost reduction, as a primary interest of adding mineral fillers to polymers, has transformed during the time into increasing demands to fulfill a functional role of polymer–matrix composites [1–3]. Since incorporated fillers and elastomers affect the structure of polymer matrix and thus change the ultimate properties of composites, the control of interactivity, dispersion, and phase morphology of ternary composites is very important for tailoring the mechanical properties.

Isotactic polypropylene (iPP) is one of the most widely used commodity thermoplastics because of its outstanding properties, in particular easy processability, recycling ability, heat distortion temperature above 100°C, versatility of applications, etc. Commonly used mineral fillers for the iPP are talc, calcium carbonate, glass beads and fibers, mica, silica, and wollastonite. Among these fillers, mineral wollastonite, $CaSiO_3$ (calcium metasilicate), is a suitable reinforcing filler for the iPP because of high aspect ratio (L/D = 10:1 ... 20:1) and to its relatively high hardness (4.5 according to Mohs) [1–3].

The incorporation of wollastonite as an inorganic filler improves some mechanical properties of the iPP, such as stiffness, hardness, and strength, but it usually reduces the toughness, leading to poor impact strength of iPP at low temperatures. This deficiency could be abolished with the addition of proper elastomers as good impact modifiers. It would be very appropriate to find suitable thermoplastic elastomers simultaneously efficient as an impact modifier and compatibilizer (elastomer with encapsulation efficiency) for the iPP composites.

Although different authors [4–6] have reported a wide spectrum of results on how wollastonite affects mechanical properties, supermolecular structure of binary iPP/wollastonite composites, as well as those modified by impact modifiers, coupling agents or compatibilizers have been

Correspondence to: Ivan Šmit; e-mail: ismit@irb.hr
contract grant sponsor: Ministry of Science, Education and Sports of the Republic of Croatia; contract grant number: 098-0982904-2955; contract grant sponsor: Ministry of Higher Education, Science and Technology of the Republic of Slovenia.
DOI 10.1002/pc.20649
Published online in Wiley InterScience (www.interscience.wiley.com).

rarely investigated. Elastomers based on ethylene copolymers [ethylene–propylene rubber (EPR), ethylene–propylene–diene rubber (EPDM), and metallocene copolymers based on ethylene] are commonly used to toughen the iPP. The addition of components such as iPP-*g*-MA or EPDM to the iPP/wollastonite composites improves impact strength and affects final morphology. It has been proved that EPDM tercopolymer preferably incorporates in the iPP matrix in the form of dispersed particles rather than it encapsulates the wollastonite filler [6]. EPDM copolymers are replaced by novel metallocene EPR copolymers with propylene being the major component (>80 wt%) [7]. These new specialty Vistamaxx™ thermoplastic elastomers are actually co/terpolymers of propylene balanced with ethylene and other α-olefins. Because of uniform intermolecular/intramolecular distribution of composition and intermediate crystallinity between the essentially amorphous EPR and the semicrystalline iPP, these P-E copolymers are tough elastomers with uniquely soft, elastic properties and superb compatibility with various polyolefins [7, 8].

The aim of our investigation was to determine the structure–mechanical property relationships of the isotactic polypropylene/wollastonite/elastomer (iPP/W/EPR) composites with incorporation of wollastonite and two metallocene EPR elastomers of different viscosity. In this article, the effect of wollastonite and EPRs on final phase structure and morphology of the iPP/W/EPR composites are discussed, while the mechanical properties and adhesion phenomena of corresponding composites will be published in a submitted paper [9].

EXPERIMENTAL

Materials

The materials used in this study were iPP, two types of wollastonite, and two types of propylene-based metallocene copolymers (EPR) with propylene being the major component. The iPP used for sample preparation was Moplen HP501L, Basell [melt flow rate (MFR) = 6 g/10 min, ρ = 0.90 g/cm^3, M_n = 120,000 g/mol]. Applied mineral fillers were proprietary (combination of silanes) surface-treated wollastonite (W1) Tremin 939 300 ZST, Quarzwerke (ρ = 2.85 g/cm^3, specific surface 1.2 m^2/g, d (50%) = 9 μm), and wollastonite surface treated with aminosilane (W2) Tremin 939 300 AST, Quarzwerke (ρ = 2.85 g/cm^3, specific surface 1.2 m^2/g, d (50%) = 9 μm). Two metallocene propylene–ethylene copolymers of Exxon Mobil with different viscosity, Vistamaxx-VM-1100 [MFR (EPR-1) = 4.5 g/10 min; ρ = 0.863 g/cm^3; M_n = 92,900; M_w/M_n = 3.4] and Vistamaxx-VM-1120 [MFR (EPR-2) = 20 g/10 min; ρ = 0.863 g/cm^3; M_n = 48,100; M_w/M_n = 2.66], were used as elastomers.

Sample Preparation

Binary iPP/wollastonite and ternary iPP/wollastonite/elastomer composites were prepared in an oil-heated Brabender kneading chamber. The iPP/wollastonite ratio was kept constant at 92/8 vol% and the elastomer of 2.5, 5, 10, and 20 vol% was added. The components were put into a chamber preheated up to 200°C with a rotor speed of 50 min^{-1}. The components were kneaded for 7 min. After homogenization, the melt was rapidly transferred to a preheated laboratory press and compression molded into 1- and 4-mm-thick plates. The pressing temperature was 220°C, pressure 10 MPa, and the pressing time of 14 min for 1-mm and 11.5 min for 4-mm-thick plates. Afterwards, the plates were cooled to room temperature in air.

Optical Microscopy

A Leica light microscope (model DMLS) with digital camera was used for thin, crossed microtomed sections (1-mm-thick plates) observation.

Scanning Electron Microscopy

A Jeol JSM-840A scanning electron microscope (SEM) was used for studying the morphology of the investigated composites. The samples were fractured in liquid nitrogen and covered with gold before being examined by a microscope. The *n*-heptane was used for etching the elastomeric phase in order to obtain better examination of distributed elastomeric particles in composites. All SEM micrographs are secondary electron images.

Transmission Electron Microscopy

Ultrathin sections (75–85 nm thick) were cut from 4-mm-thick plates with Leica-Ultracut E microtome equipment with a diamond knife. Before microtoming, samples were exposed to RuO_4 in order to contrast and harden the samples. Microtomed ultrathin sections were then collected on copper grids and micrographs were taken at an acceleration voltage of 100 kV by a Tecnai G^2 12 microscope with CCD camera (Gatan Bioscan).

Wide-Angle X-Ray Diffraction

The wide-angle X-ray diffractograms of rotated samples (1-mm-thick plates) were taken by a Philips diffractometer with monochromatized Cu Kα radiation in the diffraction range of 2θ = 5–40°. The degree of crystallinity, $w_{c,x}$, was evaluated by the Hermans–Weidinger method [10]. The crystallite size L_{110} was calculated by Scherrer formula [11] from half-maximum width of 110 α-iPP reflection, and B value (earlier known as K value) [12], as a measure for hexagonal β-form content, was calculated by formula (1) proposed by Zipper et al. [13] as

 DOI 10.1002/pc

$$B = \frac{I_{\beta-300}}{I_{\beta-300} + I_{110} + I_{040} + I_{130}} \quad (1)$$

where I represents the intensities of the corresponding reflections.

The orientation parameters A_{110} and C used as measures for orientations of corresponding (110) and (040) planes were calculated by formulae (2) and (3) proposed by Zipper et al. [13]:

$$A_{110} = \frac{I_{110}}{I_{110} + I_{111} + I_{131+041}} \quad (2)$$

$$C = \frac{I_{040}}{I_{110} + I_{040} + I_{130}} \quad (3)$$

where I represents the intensities of the corresponding reflections.

Differential Scanning Calorimetry

Thermal analysis was performed with a Perkin Elmer DSC-7 calorimeter. The samples (9.3–10.3 mg) were cut from 1-mm-thick compression-molded plates, placed in aluminium pans, and sealed. The instrument was operated in a dynamic mode. First, the samples were heated to 200°C with a controlled heating rate of 10°C/min in extra pure nitrogen environment and then kept at the same temperature for 5 min [14]. Thermograms were recorded during the cooling cycle with a cooling rate of 5°C/min to 25°C, as well as by second heating cycle to 200°C with a heating rate of 10°C/min. The melting temperatures, T_m, of samples were obtained from the maximum of the second melting peaks, and the enthalpies of melting, Δh, were obtained from the peak area and recalculated on iPP mass. The crystallinity, $w_{c,h}$, of iPP and of the composites was calculated by *Eq. 4* as

$$w_{c,h} = \frac{\Delta h}{\Delta h^0_{PP}} \times 100 \quad (4)$$

where Δh is the enthalpy of fusion per gram of the sample recalculated on iPP mass and Δh^0_{PP} is the enthalpy of fusion per gram of 100% crystalline iPP. For Δh^0_{PP} the value of 165 J/g as an average heat of fusion of the five data points were used [15].

The following quantities were given from crystallization exotherm and were related with crystallization parameters [14]:

(i) The peak temperature of the crystallization exotherm, T_c.
(ii) Slope of the exotherm, S_i, which is the slope of the high temperature side of the exotherm.

RESULTS AND DISCUSSION

Phase Morphology

Optical Microscopy. Polarization micrographs of neat iPP, binary iPP/W1, and ternary iPP/W1/EPR-2 composites in Fig. 1 represent the change of typical morphologies by introduction of filler and elastomer into the iPP matrix. The micrograph of neat iPP reveals well-developed spherulitic morphology with polygonal and irregular, radial spherulites (with average maximal spherulite diameter ~65 μm) (Fig. 1a). The incorporation of both wollastonite types into iPP matrix disturbs regular spherulitization, leading to the morphology with small irregular spherulites or with thin, dark branched iPP grains without the Maltese cross (Fig. 1b). It seems that thin needle-like

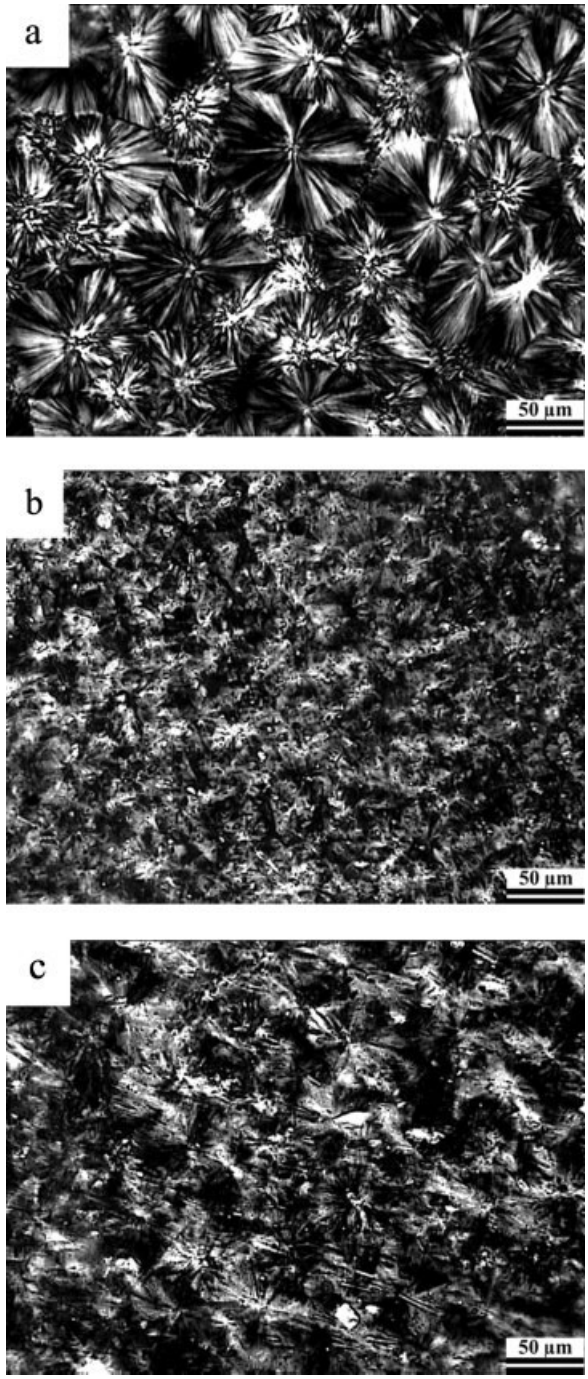

FIG. 1. Polarization micrographs of (a) neat polypropylene, (b) iPP/W1 (92/8), and (c) iPP/W1/EPR-2 (92/8 + 20 vol%) composites.

wollastonite particles strongly affect the nucleation of iPP matrix, thus hindering well-developed spherulitization in the iPP matrix. The spherulite growth may be also restrained by steric hindrances at particles surface of filler according to Burke et al. [16]. It was also shown [17] that the spherulites size abruptly decreased to approximately half with low addition of wollastonite (2 vol%); the disturbance of spherulites and the decrease of their size continuously occur with increasing content of four different types of wollastonite (up to 16 vol%). Because the spherulites were still recognizable in some of different iPP/W 92/8 composites, 8 vol% of wollastonite might be considered as an approximate limit filler amount at which the spherulitic morphology of the iPP matrix is seen [16].

Introduced elastomeric EPR particles may affect the crystallization of the iPP matrix by competitive nucleation and solidification effect, thus influencing the final morphology of the ternary composites [6, 17, 18]. The growth of spherulites in the iPP/W/EPDM composites at higher amounts of added elastomers was explained by solidification effect [6]. Polarization micrographs of presented composites with both wollastonite and EPR types exhibit the developing iPP spherulites (till $\sim$50 μm in size for composites with 20 vol% of added elastomers), as shown in Fig. 1c. These micrographs also reveal high level of parallel orientation of wollastonite particles. The enlarging of the spherulites with addition of higher EPR amounts seems to be caused by different factors in solidification process that prevail the nucleation ability of wollastonite.

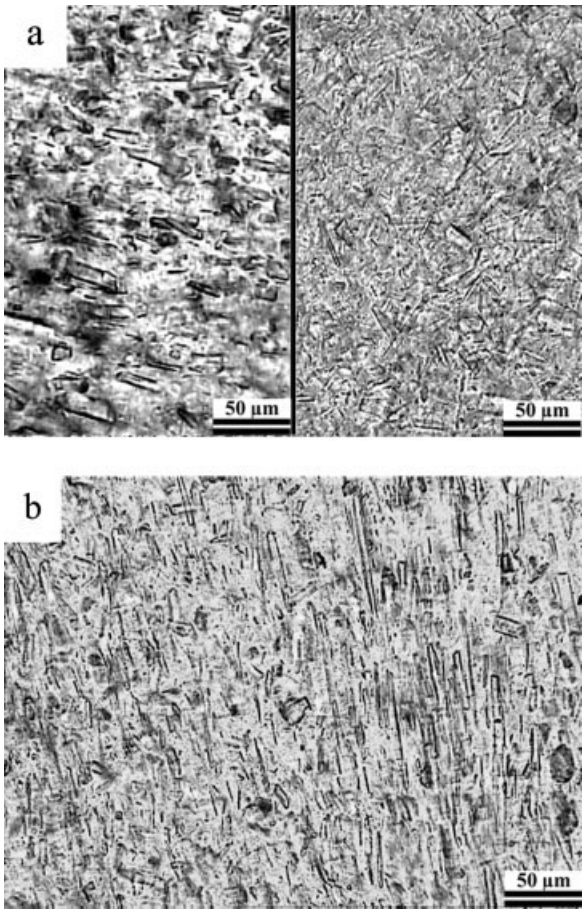

FIG. 2. Optical micrographs of (a) iPP/W2 92/8 and (b) iPP/W2/EPR-2 (92/8 + 20 vol%) composites.

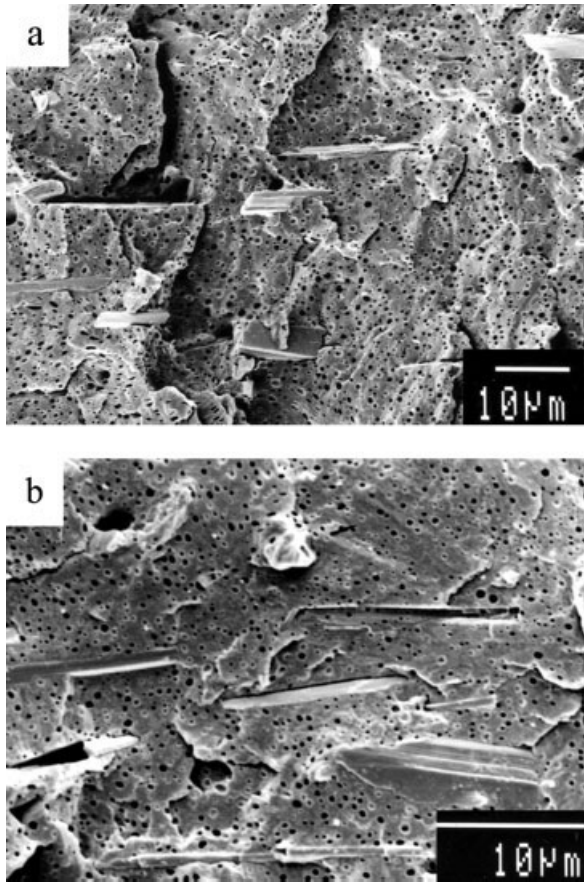

FIG. 3. SEM micrographs of (a) iPP/W2/EPR-1 (92/8 + 20 vol%) and (b) iPP/wollastonite/EPR-2 (92/8 + 20 vol%) composites.

All micrographs under cross and parallel polarizers of all composites reveal homogenous distribution of separated wollastonite particles without agglomeration (see Fig. 2). Needle-like wollastonite particles in binary iPP/W composites orientate preferentially plane-parallel to the compression-molded surface and the degree of its orientation varies somewhat through the sample (Fig. 2a). The addition of both EPRs to the iPP/W composites increases this plane-parallel orientation (Fig. 2b). This effect differs from the effect of SEBS and SEBS-*g*-MA elastomers that maintain or even decrease plane-parallel orientation of wollastonite particles [19].

Scanning Electron Microscopy. Scanning electron micrographs of fractured iPP/wollastonite composites with 20 vol% of added EPR-1 and EPR-2 are presented in Fig. 3a and b. They confirm the homogeneous distribution of wollastonite particles and also reveal the homogeneously dispersed spherical EPRs particles in the iPP matrix.

DOI 10.1002/pc

Acicular wollastonite particles orientate preferentially in the melt flow direction during the compression molding of the sample into a plate. Both micrographs reveal the presence of the wollastonite crystals with higher plane-parallel orientation as well as the lesser number of hollows from which wollastonite particles are pulled out at the etched surface of the ternary composites (Fig. 3a and b). Dispersed EPR-2 particles are smaller than EPR-1 particles (note the different magnification in the micrographs shown in Fig. 3a and b) probably because of different viscosity of elastomers. Less number of spherical EPR particles seems to be located randomly at the surface of wollastonite particles.

Transmission Electron Microscopy. Ternary polymer–matrix composites exhibit two typical microphase morphologies with respect to location of filler and elastomer particles to each other in the polymer matrix [20]: (i) separated microphase morphology where elastomer and filler particles are randomly dispersed in the polymer matrix (apart from each other), and (ii) core-shell morphology where the filler particles are encapsulated by the elastomer. However, the most frequent morphology observed for various composites consists of a combination of two main morphologies [20]. TEM micrographs in Fig. 4 revealed significant prevalence of separated microphase morphology in ternary iPP/W/EPR composites. TEM micrographs of the iPP/W2/EPR-1 composites with lower (Fig. 4a) and higher magnification (Fig. 4b) show prevalently separated spherically dispersed EPR-1 particles and lesser number of EPR-1 particles randomly accommodated at the surfaces of wollastonite particles. The composites with EPR-2 (Fig. 4c) reveal lower encapsulation ability than composites with EPR-1 elastomer. The morphology of composites with EPR-1 is similar to the morphology of iPP/W/SEBS composites [19]. Generally, encapsulation ability of EPRs is significantly lower than that of styrenic rubber block copolymers [19]. Obviously, the encapsulation of wollastonite particles by EPRs was not affected neither by the conditions during the preparation of the composites [21] nor by the unsaturated (like SBS, SIS) or polar (like SEBS-*g*-MA) nature of elastomers as a compatibilizer [22]. As a result the degree of core-shell morphology is negligible. Higher micrographs magnification of composites with EPR-1 and EPR-2 (Fig. 4b and c) reveal spherical form of dispersed EPR particles without formation of any EPR interlayer. Furthermore, typical micrograph of spherical dispersed EPR particle with higher magnification shown in Fig. 4b exhibits the protrusion of polypropylene lamellae (white strings) through the black EPR sphere. This could be a result of good compatibility of dispersed EPR particles with iPP matrix or even partial cocrystallization ability of the iPP and EPR chains at supermolecular level [7, 17]. This result is in good accordance with spherulite growth by incorporation of EPR elastomers observed in polarization micrographs of composites with 20 vol% of elastomer (Fig. 1c). The addition of EPR elastomers might prolong the crystallization of the iPP matrix, and thus enable easier transfer of the iPP chains (or even EPR chains) from the melt into growing iPP lamellae, enhancing spherulite growth.

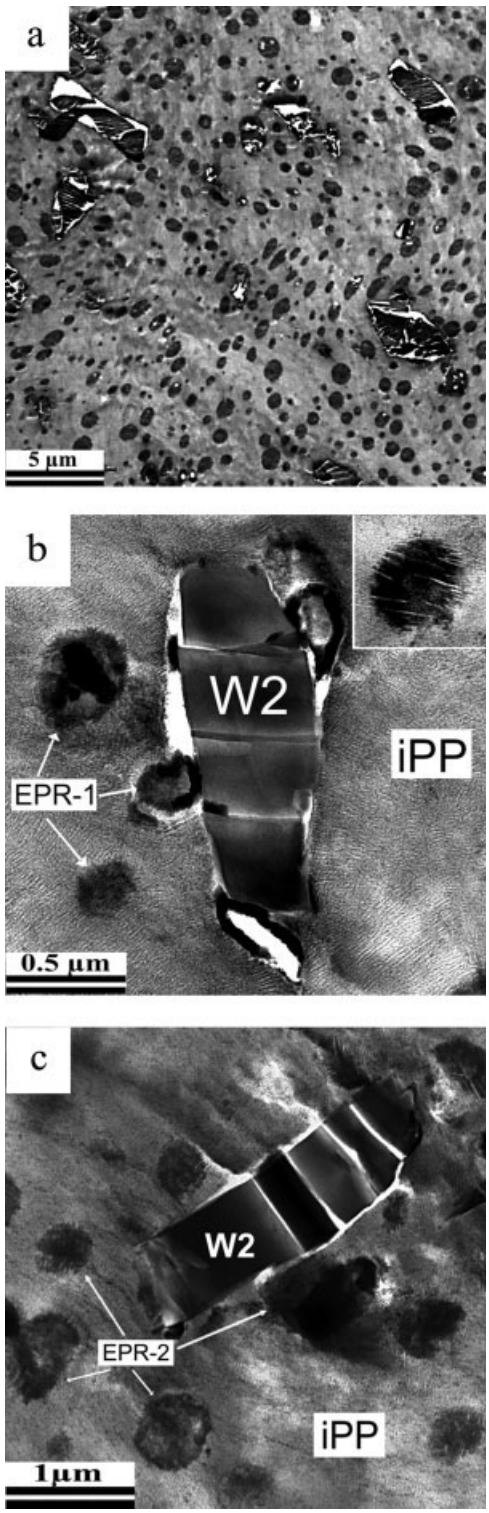

FIG. 4. TEM micrographs of iPP/W2/EPR-1 (92/8 + 20 vol%) composite at (a) lower and (b) higher magnification, and (c) iPP/wollastonite/EPR-2 (92/8 + 20 vol%) composite.

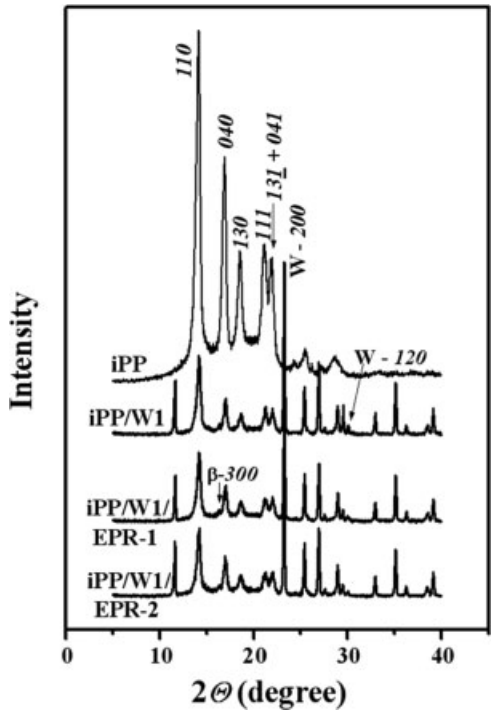

FIG. 5. Diffractograms of the iPP, binary iPP/W1 92/8 composite, and ternary composites with 20 vol% of EPR-1 and EPR-2 copolymers.

Phase Characteristics

Phase Structure. WAXD curve of neat iPP exhibits solely monoclinic α-form, whereas, apart from α-form, X-ray diffractograms of composites reveal small amounts of hexagonal β-form of crystalline iPP phase as shown by the β-300 peak in Fig. 5. Wollastonite is known as a strong β-nucleator for the iPP [23]. Relatively low content of β-phase in the presented iPP/W composites (with B or K values for measuring β-form content being 0.041–0.051), in comparison to the iPP/W composites presented in the paper of Liu et al. [23] ($K = 0.14$ for composite with 3.2% of wollastonite), might arise because both types of wollastonite particles (W1 and W2) are overlapped by (alkyl)(amino)silane layers. The addition of both EPR copolymers to the binary iPP/W composites does not affect the nucleation of β-iPP form (varying of B values from 0.036 to 0.051 could be considered as error inside limit resolution of the applied method). This fact is in good accordance with negligible degree of core-shell morphology revealed by TEM.

Diffractograms of both applied wollastonites are close to the Card No. 27-1064 [triclinic cell with space group P$\bar{1}$ (2T)] [24].

Crystallinity and Crystallite Size. The overall degree of crystallinity has been calculated as overall crystalline fraction (α- plus β-iPP phase) for the total polymer fraction (iPP plus EPR) in ternary composite following the Hermans–Weidinger method [10]. The crystallinity calculation has taken into account the total polymer fraction (iPP plus EPR), because the main broad diffraction maximum is the common maximum of two overlapping broad maxima of the iPP and EPR amorphous phases in the diffraction angle range of $2\theta = 7$–32°. The crystallinity values are recalculated on the pure iPP, in order to compare them with those obtained from the enthalpy of fusion per gram of the sample recalculated on iPP mass. The evaluated crystallinity values, $w_{c,x}$, increase to some extent upon the incorporation of wollastonite filler in pure iPP (see Fig. 6). This effect is in accordance with the observation referred by Wypich [3]. The crystallinity also increases with the increase of EPR elastomers content and this increase could be presented by multiple fitting line (see Fig. 6). The increase of the β-iPP content due to the β-nucleation ability of wollastonite obviously contribute to the increase of crystallinity in binary iPP/W composites. However, the increase of crystallinity with increasing EPR content could be explained by several additional effects: (i) the most influenced seems to have enhanced or prolonged crystallization because of partial miscibility and solidification effect of EPR elastomer, (ii) dissolution of amorphous iPP and EPR phases by wollastonite, and (iii) limiting resolution of applied method.

The crystallite size, L_{110},exhibits steady increase by introduction of wollastonite as well as with the addition of EPRs to the iPP matrix, as shown in Fig. 7. It is interesting that the L_{110} values for all composites with 20 vol% of EPRs are very similar. A steady increase of the L_{110} crystallite size upon EPR increase might be ascribed to the solidification effect, which prolongs the crystallization of the iPP matrix, and to the enhanced crystallization because of partial miscibility of the iPP and EPR chains; both effects enable easier migration of iPP chains transferred by EPR melt during the crystallization process.

Orientation. A_{110} and C parameters, as an orientation measure for α-form crystallites in plane-parallel to the

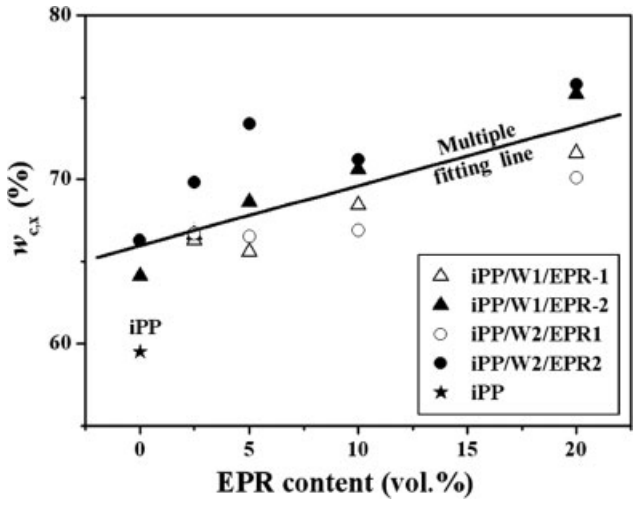

FIG. 6. Overall degree of crystallinity, $w_{c,x}$, of composites recalculated on polypropylene mass unit as a function of the EPR content.

DOI 10.1002/pc

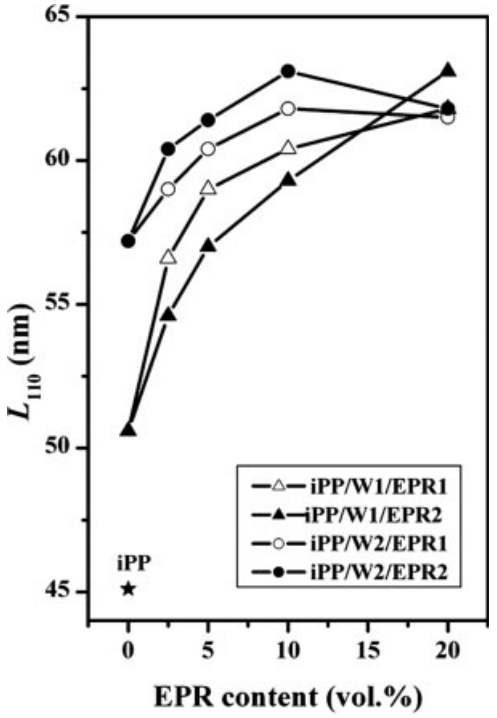

FIG. 7. Crystallite size, L_{110}, as a function of the EPR content.

sample surface, are presented in Figs. 8 and 9. The incorporation of wollastonites and small amounts of EPR elastomers to the iPP matrix increases somewhat the A_{110} values (maximum at 5 vol% of EPR in Fig. 8) and decreases the C values (minimum at 5 vol% of EPR in Fig. 9). Similarly, but significantly, stronger behavior of A_{110} and C parameters observed in the iPP/W/SEBS-*g*-MA composites [17] was explained by the decreased influence of wollastonite on the orientation of α-iPP crystallites because of the encapsulation of wollastonite particles by polar SEBS-*g*-MA elastomer. The increase of the A_{110} parameter (to ~0.7) upon addition of EPRs indicates the increased number of (110) planes in plane-parallel to the sample surface. On the other hand, the lowering of the C parameter values (up to ~0.175) might be explained, according to Zipper et al. [13], by maintaining either *c*-axial orientation or isotropic iPP matrix ($0 < C \ll 1$ for pure *c*-axis orientation or for isotropic material). According to Fujiyama et al. [25], *c*-axis-oriented lamellae imply orientation of macromolecular *c*-axis, lying in plane-parallel to the sample surface in machine direction.

Thermal Properties. DSC traces of second heating cycles exhibit negligible variation of peak temperature of melting endotherm (from 163.9 to 165.8°C) of α-iPP crystallites with incorporation of wollastonite and EPRs into the iPP matrix (approximately melting peak is $T_m \sim$ 165°C). Obviously, neither wollastonite fillers nor EPR elastomers affect significantly the melting peak temperature of α-iPP. The degree of crystallinity, $w_{c,h}$, obtained from the DSC melting peak behaves quite similar to that,

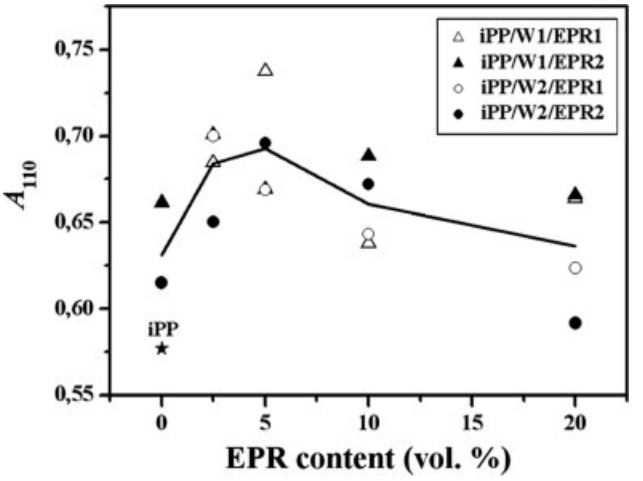

FIG. 8. Orientation A_{110} parameter as a function of the EPR content.

$w_{c,x}$, calculated from WAXD diffractograms. Increasing multiple fitting line of the $w_{c,h}$ values exhibits only somewhat lower slope than that for $w_{c,x}$ (0.616 for $w_{c,h}$ in comparison to 0.700 for $w_{c,x}$ in Fig. 6).

The influence of both wollastonite and EPR elastomers on the crystallization of iPP matrix has been deduced from the crystallization exotherms. The incorporation of both wollastonites and EPR elastomers affects somewhat the profile of crystallization exotherm in the same way. The incorporation of both wollastonites and EPR elastomers enhances somewhat the asymmetry of crystallization exotherm, thus decreasing the initial slope and shifting the peak of crystallization exotherm to the higher temperature. Both wollastonites slightly increase the crystallization temperature values, T_c, of the α-iPP matrix (see Fig. 10). Such decrease in supercooling (the increase of the T_c values) correlates with the increase of β-iPP phase content nucleated by wollastonite. This fact is in a good agreement with the finding of Fujiyama that the crystallization temperature increases with an increase in β-iPP content (actually with γ-quinocridone content) [26]. Low

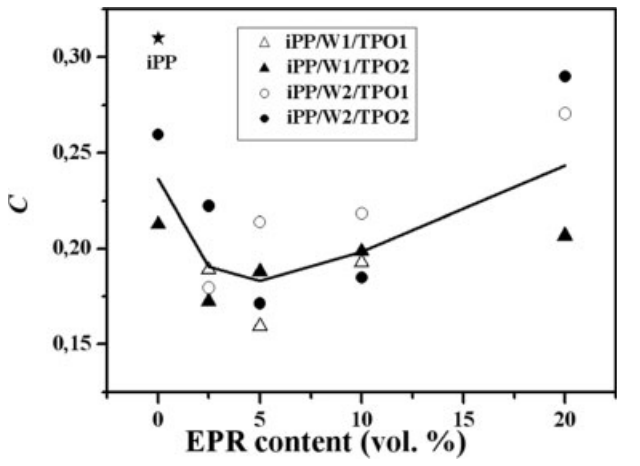

FIG. 9. Orientation C parameter as a function of the EPR content.

EPR amount (2.5 vol%) additionally increases the T_c values, but further addition of EPRs affects T_c values negligibly (see Fig. 10). The increase of crystallization temperature is usually connected with the increase of heterogeneous nuclei. Bartczak et al. have concluded from summarized data in a review [27] that in partially miscible iPP blends with elastomers (like EPR and EPDM) the number of primary nuclei increased with increasing elastomer content. The impurities migrate from elastomer phase (EPR, EPDM) toward the iPP matrix during the preparation of blend by melt-mixing and they act as heterogeneous nuclei [27]. As a result of increased nuclei density the crystallization of the iPP begins at higher temperature by cooling the melt (see Fig. 10). The decrease in supercooling ($\Delta T = T_m - T_c$) due to the introduction of wollastonite and EPRs may reflect on the crystallization rate of the iPP matrix. The slope values of exotherm, S_i, as a measure for nucleation rate [14], decrease with the incorporation of wollastonites and EPR elastomers (see Fig. 11); they behave quite symmetrically opposite to the T_c values shown in Fig. 10. Obviously, the decrease in supercooling, ΔT (the increase of T_c values in Fig. 10), manifests in slower overall crystallization of the iPP matrix (see Fig. 11). This fact is in accordance with the observed higher crystallization half-life of polypropylene blends with metallocene linear low-density polyethylene than with pure PP at the same isothermal crystallization temperature [28].

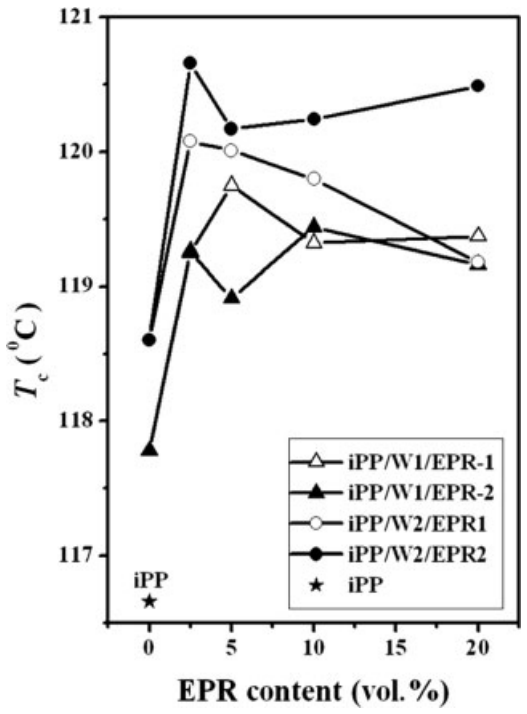

FIG. 10. Crystallization temperature (T_c) as a function of the EPR content.

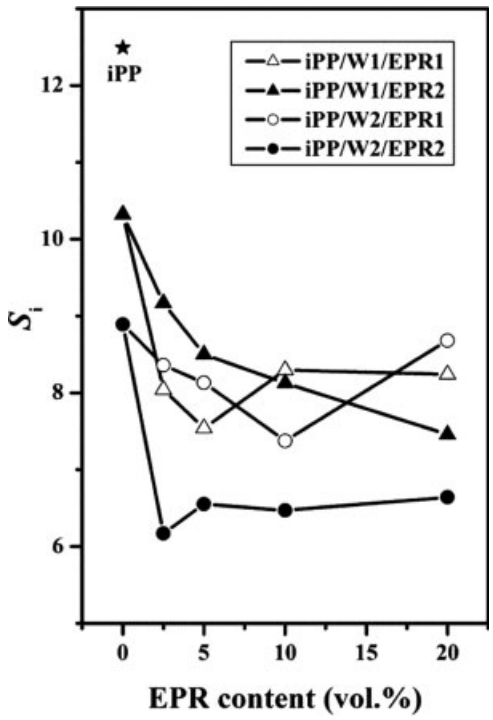

FIG. 11. Slope of the exotherm (S_i) of composites as a function of EPR content.

CONCLUSION

Wollastonite and dispersed EPR particles, homogeneously incorporated into the iPP matrix, affected the final supermolecular structure (phase structure and morphology) of the iPP/wollastonite/EPR composites. The wollastonite particles were orientated plane-parallel to the sample surface and disturbed the well-developed spherulitization of iPP. Both EPRs enhanced plane-parallel orientation of wollastonite particles and affected the crystallization of iPP matrix. EPR elastomers, as a compatible or even partial miscible or cocrystallizable with the iPP, strongly enhanced the spherulite and crystallite growth, and consequently the degree of crystallinity. The investigation on phase morphology has shown significant prevalence of separated microphase morphology in ternary iPP/wollastonite/EPR composites. Such prevalence of separation over core-shell morphology seems to be the result of prevalence of the iPP-EPR interactions because of constitution similarity of P-E and iPP chains over the EPR-wollastonite interactions. According to this fact, metallocene EPR elastomers would be rather efficient impact modifiers than encapsulation compatibilizers for the iPP/wollastonite composites.

ACKNOWLEDGMENTS

The authors thank Mr. J. Pohleven for his help in the experimental work, and Dr. E. Ingolič for her valuable help in elaborating the TEM micrographs.

 DOI 10.1002/pc

REFERENCES

1. J.H. Kietzman, "Asbestiform Fillers," in *Additives for Plastics, Vol. 1*, R.B. Seymour, Ed., Academic Press, New York, **51** (1978).
2. R.N. Rothon, *Adv. Polym. Sci*., **139**, 67 (1999).
3. G. Wypich, *Handbook of Fillers*, SPE, New York, **167** (1999).
4. D.H. Roberts, "Chemical Coupling of Polypropylene Systems Containing Non-Glass Fillers," in *Proceedings of SPE ANTEC*, Atlanta, USA, 1427 (1998).
5. J. Chu, C. Xiang, H.-J. Sue, and R.D. Hollis, *Polym. Eng. Sci*., **40**, 944 (2000).
6. I. Šmit, V. Musil, and I. Švab, *J. Appl. Polym. Sci*., **91**, 4072 (2004).
7. Exxon Mobil, "VISTAMAXX^{TM} Specialty Elastomers, Innovative Elastomeric Solutions from ExxonMobil Chemical," *General Technical Overview*, K04, Machelen, Belgium (2004).
8. C. Cheng, G. Racine, S. Srinivas, and S. Datta, "Novel Propylene-Based Specialty Elastomers: Structure and Properties," in *Proceedings of SPE ANTEC*, Chicago, USA, 4220 (2004).
9. I. Švab, V. Musil, A. Pustak, and I. Šmit, *Polym. Comp*., submitted.
10. P.H. Hermans and S.A. Weidinger, *Makromol. Chem*., **50**, 98 (1961).
11. L.E. Alexander, *X-Ray Diffraction Methods in Polymer Science*, Wiley, New York, **423** (1969).
12. A. Turner-Jones, J.M. Aizlewood, and D.R. Becket, *Makromol. Chem*., **75**, 134 (1964).
13. P. Zipper, A. Janosi, E. Wrentschur, C. Knabl, and P.M. Abuja, *Österr. Kunststoff-Zeitschrift*, **24**, 162 (1993).
14. A.K. Gupta and S.N. Purwar, *J. Appl. Polym. Sci*., **29**, 1595 (1984).
15. B. Wunderlich, *Macromolecular Physics, Vol. 3: Crystal Melting*, Academic Press, New York, Chapter 8, **63** (1980).
16. M. Burke, R.J. Young, and J.L. Stanford, *Plast. Rubber Compos. Process. Appl*., **20**, 121 (1993).
17. I. Švab, "The Study of Modification of Isotactic Polypropylene with Wollastonite and Elastomers," Ph.D. Thesis, University of Maribor, Maribor, Slovenia (2006).
18. W. Wenig and A. Wasiak, *Colloid Polym. Sci*., **271**, 824 (1993).
19. I. Švab, V. Musil, T. Jurkin, and I. Šmit, *Polym. Eng. Sci*., **47**(**12**), 2145 (2007).
20. Y. Long, R.A. Shanks, and Z.H. Stachursky, *Prog. Polym. Sci*., **20**, 651 (1995).
21. Y.C. Ou, T.T. Guo, X.P. Fang, and Z.Z. Yu, *J. Appl. Polym. Sci*., **74**, 2397 (1999).
22. J.E. Stamhuis, *Polym. Compos*., **9**, 280 (1988).
23. J. Liu, X. Wei, and Q. Guo, *J. Appl. Polym. Sci*., **41**, 2829 (1990).
24. *Powder Diffraction File*, Card No. 27-1064, ICDD, JCPDS, Swarthmore, PA.
25. M. Fujiyama, T. Wakino, and Y. Kawasaki, *J. Appl. Polym. Sci*., **35**, 29 (1988).
26. M. Fujiyama, *Int. Polym. Process*., **10**, 172, 251 (1995).
27. Z. Bartczak, E. Martuscelli, and A. Galeski, "Primary Spherulite Nucleation in Polypropylene-Based Blends and Copolymers," in *Polypropylene: Structure Blends and Composites, Vol. 2: Copolymers and Blends*, J. Karger-Kocsis, Ed., Chapman and Hall, London, Chapter 2, 25 (1995).
28. M. Razavi-Nouri, *Polym. Test*., **26**, 108 (2007).